

The Emperor Seamounts: Southward Motion of the Hawaiian Hotspot Plume in Earth's Mantle

John A. Tarduno,^{1*} Robert A. Duncan,² David W. Scholl,³ Rory D. Cottrell,¹ Bernhard Steinberger,⁴ Thorvaldur Thordarson,⁵ Bryan C. Kerr,³ Clive R. Neal,⁶ Fred A. Frey,⁷ Masayuki Torii,⁸ Claire Carvallo⁹

¹Department of Earth and Environmental Sciences, University of Rochester, Rochester, NY, USA. ²College of Oceanic and Atmosphere Science, Oregon State University, Corvallis, OR, USA. ³Geophysics Department, Stanford University, Stanford, CA, USA. ⁴Institute for Frontier Research on Earth Evolution, Japan Marine Science and Technology Center, Yokosuka, Japan. ⁵Department of Geology and Geophysics/SOEST, University of Hawaii, Honolulu, HI, USA. ⁶Department of Civil Engineering and Geological Sciences, University of Notre Dame, Notre Dame, IN, USA. ⁷Department of Earth, Atmospheric and Planetary Sciences, MIT, Cambridge, MA, USA. ⁸Department of Biosphere-Geosphere System Science, Okayama University of Science, Okayama, Japan. ⁹Department of Physics, Geophysics Division, University of Toronto, Mississauga, Canada.

*To whom correspondence should be addressed. E-mail: john@earth.rochester.edu

The Hawaiian-Emperor hotspot track has a prominent bend that has been interpreted to record a change in plate motion traced by the Hawaiian hotspot fixed in the deep mantle. However, paleomagnetic and radiometric age data from samples recovered by ocean drilling define an age-progressive paleolatitude history indicating that the Emperor Seamount trend was principally formed by the rapid (over 40 mm yr⁻¹) motion of the Hawaiian hotspot plume during Late Cretaceous to Early Tertiary times (81-47 Ma). Evidence for motion of the Hawaiian plume affects models of mantle convection and plate tectonics, changing our understanding of terrestrial dynamics.

The concept of an age-progressive set of volcanic islands, atolls and seamounts produced by a hotspot plume fixed in the deep mantle was first developed to explain the Hawaiian Islands (1). The bend separating the westward-trending Hawaiian island chain from the northward trending Emperor seamounts is most often interpreted as an example of a change in plate motion recorded in a fixed-hotspot frame of reference (2).

However, global plate circuits suggest large relative motions between Hawaii and hotspots in the Atlantic and Indian Oceans (3–6). Improved mapping of marine magnetic anomalies in the Pacific has failed to define direction at 43 Ma (7) that would be expected if such a large change in plate motion had occurred. There is also a general lack of circum-Pacific tectonic events (8) at this time. Recent age data suggest a somewhat older age for the bend [~47 Ma (9)], but this revised timing still does not correspond to an episode of profound plate motion change recorded within the Pacific basin, or on its margins.

One approach to examine hotspot fixity is to determine the age and paleolatitude of volcanoes that form a given hotspot track. For the Hawaiian hotspot, the paleolatitudes of extinct volcanic edifices of the Emperor chain should match the present-day latitude of Hawaii (~19° N) if the hotspot has remained fixed with respect to Earth's spin axis. The most

reliable indicators of paleolatitude are basaltic rocks, but enough time must be spanned by any section such that geomagnetic secular variation is sampled. Recovery of such samples requires ocean drilling technology, and only a few seamounts have been sampled to date.

Paleomagnetic analyses of 81-million-year-old basalt recovered from Detroit Seamount (Site 884) yielded a paleolatitude of ~36° N (10) that is discordant with Hawaii. Data from ~61 million-year-old basalt (9) from Suiko Seamount define a paleolatitude of 27° N (11). These data suggest that the Emperor Seamounts record southward motion of the hotspot plume in the mantle (10).

A Paleomagnetic Test. Ocean Drilling Program (ODP) Leg 197 (12) sought to test the hypothesis of southward motion of the Hawaiian hotspot by drilling additional basement sites in the Emperor chain (Fig. 1). We collected detailed stepwise alternating field demagnetization (AF) data aboard the drilling ship *JOIDES Resolution*. Although these shipboard data are of high resolution, they alone are insufficient to define paleolatitudes. Magnetic minerals with intermediate to high coercivities, carrying magnetizations resistant to AF demagnetization, are commonly formed during subaerial or seafloor weathering. The magnetizations of these mineral phases are easily resolvable in thermal demagnetization data which we also discuss here (14).

The geomagnetic field at a radius r , colatitude θ and longitude ϕ can be described by the gradient of the scalar potential (Φ):

$$\Phi(r, \theta, \phi) = r_e \sum_{l=1}^{\infty} \sum_{m=0}^l \left(\frac{r_e}{r}\right)^{l+1} \times P_l^m(\cos\theta)[g_l^m \cos m\phi + h_l^m \sin m\phi]$$

where P_l^m are partially normalized Schmidt functions, r_e is the radius of the Earth and the Gauss coefficients g_l^m and h_l^m describe the size of spatially varying fields. At least several

millenia must be sampled such that the axial dipole term (g_0^1) becomes dominant, allowing an estimate of the paleolatitude.

We use the angular dispersion of inclination averages (15) from independent lava flows (inclination groups) and compare this with global lava data of the same age (16) to examine whether secular variation has been adequately sampled (14, 17). Observations of the physical aspects of the lava flows, as well as petrologic and geochemical data are used to group cooling units into lava units (12, 14).

Marine sediments can also provide useful paleolatitude information, but they generally provide only minimum values of paleolatitude because of potential compaction-induced inclination flattening (18). Sediment magnetizations, however, can record significant time intervals. Similarly, chemical remanent magnetizations (CRM), carried by minerals formed during weathering, can preserve stable magnetizations that provide insight into the time-averaged field.

Koko Seamount (Site 1206). Site 1206 (Fig. 1) was positioned on the southeastern side of the lower summit terrace on Koko Seamount using crossing underway seismic profiles (fig. S1). The base of the thin sediment cover contains nannofossils of Zones NP14 and NP15, which provide an early to middle Eocene minimum age for the volcanic basement [43.5-49.7 Ma, (19)]. Fifteen volcanic formations (including pahoehoe flows, flow foot breccias and subaerial a'a units) were recovered in 278 m of basement penetration [12]. Thin intercalations of limestone, volcanoclastic sandstone and a deeply weathered flow top were also recovered, providing geological evidence of time between lava flow units. The lavas are mainly of tholeiitic composition, although two alkalic flows were noted. Plateaus in $^{40}\text{Ar}/^{39}\text{Ar}$ incremental heating spectra from six whole rock samples yield a mean age of 49.15 ± 0.21 Ma (2σ uncertainty quoted; table S1).

Reflected light microscopy revealed relatively fresh titanomagnetite grains in the lavas (fig. S2A). AF demagnetization of basalt samples ($n = 74$) showed the removal of a small low-coercivity component, followed by the definition of a characteristic remanent magnetization (ChRM) (12). Two normal polarity intervals were defined, separated by a thin reversed polarity zone; the radiometric age data are most compatible with the chron 21n-21r-22n sequence. This assignment is confirmed by thermal demagnetization ($n = 113$) which revealed univectorial decay after the removal of a small overprint (fig. S2, B and C).

Seventeen inclination groups were identified in the thermal demagnetization data (table S2) having a mean ($I_T = 38.3^\circ_{+6.9^\circ -9.3^\circ}$; hereafter all uncertainty regions are 95% confidence interval unless otherwise noted) nearly identical to that isolated by AF treatment ($I_{AF} = 38.5^\circ_{+8.4^\circ -10.9^\circ}$, based on fourteen inclination groups sampled) (fig. S2D). The angular dispersion of the thermal data ($S_F = 15.3^\circ_{+4.3^\circ -2.7^\circ}$) is within error of that predicted by global 45-80 Ma lava flows (16). Comparison of the inclination units based on thermal demagnetization with a synthetic Fisher (20) distribution (Fig. 2) suggests that the basalt sequence represents well the time-

averaged geomagnetic field. Furthermore, we note that a stable magnetization carried by hematite (likely a CRM with unblocking temperatures $T_{UB} > 580^\circ\text{C}$) in samples of the deeply weathered basalt yield a mean inclination ($I_T = 38.2^\circ_{+5.1^\circ -5.6^\circ}$, $n = 10$) that is indistinguishable from that of the lava flows.

Nintoku Seamount (Site 1205). Site 1205 on Nintoku Seamount (Fig. 1) was selected using two crossing seismic profiles which defined a ~ 43 m-thick sedimentary sequence above a flat igneous basement, on the northwestern edge of the summit region (fig. S1). Nannofossils of Zone NP10 in sediment immediately overlying basement provide a minimum age [53.6-54.7 Ma, (19)] similar to that obtained by radiometric dating of basalt from nearby Deep Sea Drilling Project (DSDP) Site 432 [56.2 ± 0.6 Ma; 1σ error; (21)].

A sequence of 25 subaerially-erupted a'a and pahoehoe lavas and interbedded sediment and soil horizons were recovered in 283 m of basement penetration (12). Two flows of tholeiitic basalt are intercalated within the lower part of the sequence, which is otherwise composed of alkalic basalt. Plateaus in $^{40}\text{Ar}/^{39}\text{Ar}$ incremental heating spectra from 6 whole-rock basalt samples (table S1) spanning the section give a mean age of 55.59 ± 0.25 Ma.

The recovered basalt contains fresh to slightly altered titanomagnetite grains (fig. S2E). AF demagnetization ($n = 144$) defined a reversed polarity magnetization after the removal of a normal polarity overprint. Biostratigraphic and radiometric age constraints indicate the basalt was erupted during chron 24r (19). Thermal demagnetization of basalt samples ($n = 85$) in general showed univectorial decay after the removal of a small overprint (fig. S2F). Unblocking temperatures sometimes extended to 625°C , indicating the presence of some hematite. Low unblocking temperatures ($< 325^\circ\text{C}$) were seen in other samples, indicating the dominance of high-Ti titanomagnetite carriers (fig. S2G) (14).

The thermal demagnetization data (twenty-two inclination groups) yield a mean ($I_T = -44.3^\circ_{+10.3^\circ -6.3^\circ}$) (table S3) that is similar to that of the AF data ($I_{AF} = -45.7^\circ_{+10.5^\circ -6.3^\circ}$) (fig. S2H). The estimated angular dispersion of the thermal data ($S_F = 19.9^\circ_{+4.8^\circ -3.2^\circ}$) is higher than predicted by models (16) based on average data from 45-80 Ma lavas, and may point to higher frequency changes in secular variation with time. Nevertheless, the geologic evidence for time, together with a comparison of the data versus a Fisherian distribution (Fig. 2), suggests the mean value represents the time-averaged field.

Detroit Seamount (Site 1204). Site 1204 (Fig. 1) was chosen along two crossing seismic profiles which revealed a flat basement surface beneath ~ 850 m of sediments (fig. S1). Two holes were drilled (A and B), penetrating 60 and 138.5 m of basalt, respectively. Diamictite and volcanic ash-rich sediment directly overlying basement contain Campanian nannofossils (CC22/23) ~ 73 -76 Ma (20); nannofossils of this zone were also recovered in a sediment interbed in the last core from Hole B, suggesting the entire basement section drilled is of this age (12).

The basement units are pillow lavas consisting of multiple lobes (that are sometimes separated by calcareous sediment) intercalated with a 46-m-thick interval of massive lava (diabase) and a 10-m-thick hyaloclastite lapilli breccia interval (12). The basalt has undergone low temperature alteration, consistent with late stage seafloor weathering. $^{40}\text{Ar}/^{39}\text{Ar}$ incremental heating spectra from 4 whole-rock basalt samples and a feldspar separate failed to show plateaus in the step-heating ages. Total fusion apparent ages range from 33 to 58 Ma indicating variable loss of radiogenic ^{40}Ar (table S1).

Reflected light microscopy showed a dominance of titanomaghemite in basalt samples (fig. S2I). Linear decay during AF demagnetization was observed in only ~ 70% of the samples examined (Hole A: $n = 9$; Hole B: $n = 39$). In these cases a normal polarity magnetization was defined (12). Thermal demagnetization, however, revealed a clear two component structure in many samples (14). A reversed polarity component was defined at low unblocking temperatures ($T_{UB} = 100^\circ\text{C} - 275\text{--}350^\circ\text{C}$) while a normal polarity component was defined at higher temperatures (fig. 2J,K). We interpret the high T_{UB} component as the primary magnetization because it is the only magnetization seen in the least altered rocks after the removal of viscous components; we believe the reversed polarity component is a later magnetization carried by titanomaghemite.

We identify only a single inclination unit in Hole A. Thermal demagnetization data ($n = 10$) yield a mean inclination ($I_T = 64.5^\circ \text{ }^{+10.2^\circ}_{-19.0^\circ}$) that differs from that observed by AF treatment ($I_{AF} = 55.5^\circ \text{ }^{+6.8^\circ}_{-8.3^\circ}$) presumably because the latter fails to separate the two components of magnetization. Based on a lithofacies succession in Hole B (12), we identify 5 inclination groups. Our thermal results ($n = 36$) indicate a mean inclination of $60.1^\circ \text{ }^{+5.2^\circ}_{-5.5^\circ}$, ($I_{AF} = 58.9^\circ \text{ }^{+5.8^\circ}_{-6.4^\circ}$, based on AF data) for Hole B (table S4, fig. S2L). Angular dispersion estimates are low ($S_F = 3.1^\circ \text{ }^{+2.0^\circ}_{-0.9^\circ}$), and at face value suggest that the sequence does not adequately sample secular variation (Fig. 2). However, we note that rather than random directions, AF and thermal demagnetization of breccia samples often revealed a consistent normal polarity direction, similar to that of the basalt flows. This observation, together with the presence of titanomaghemite, suggests that CRM's might be important at this site.

Detroit Seamount (Site 1203). Site 1203 (Fig. 1) on Detroit Seamount was located in an area of flat basement imaged in three crossing seismic lines (fig. S1). A thick (462 m) pelagic sedimentary sequence overlies basement. Eighteen compound lava flow units and 14 volcanoclastic sedimentary interbeds were drilled in 453 m of basement penetration (12). Nannofossils of Zone CC22 were identified in sedimentary beds within the basement sequence, indicating an age of 75–76 Ma (12). Plateaus in $^{40}\text{Ar}/^{39}\text{Ar}$ incremental heating spectra from 3 whole-rock basalt samples and 2 feldspar separates (table S1) yield a mean age of 75.82 ± 0.62 Ma.

The upper part of the basement sequence is nonvesicular pillow lavas and thick sparsely vesicular pahoehoe lava

flows. These lavas were deposited far from eruptive centers at relatively shallow depths (fig. S1). The lower part of the sequence is dominated by highly vesicular compound pahoehoe lavas (up to 65 m thick) but also contains pillow lavas and hyaloclastite, indicative of shallow marine to subaerial environments. Tholeiitic to transitional basalt dominates the section, but some alkali basalt is intercalated in the lower sequence. This occurrence of alkalic lavas is unexpected; it may indicate the interfingering of volcanoes in different stages of evolution, as can be seen today between Mauna Loa and Mauna Kea on Hawaii.

The lavas have a range of magnetic mineralogies, from relatively fresh titanomagnetite to grains showing titanomaghemitization (fig. S2M). AF demagnetization of most of the basalt ($n = 199$) and sediment ($n = 34$) samples examined showed a stable single component of normal polarity after removal of a low coercivity (<10 mT) overprint (12). In the two uppermost flows, AF demagnetization patterns were more complex, indicating the presence of additional, unresolved components. Titanomaghemite, detected by reflected light microscopy, is common in the upper flows.

Thermal demagnetization data of lava ($n = 87$) (fig. S2N) and sediment samples ($n = 28$) (fig. S2O) mostly showed univectorial decay after the removal of a small overprint at low unblocking temperatures. In the two uppermost flows of the sequence, however, a distinct reversed component of magnetization was isolated ($T_{UB} = \sim 100^\circ\text{C}$ to $250\text{--}325^\circ\text{C}$), before definition of a normal polarity magnetization at higher temperatures. As in the Site 1204 basalts, we interpret the higher T_{UB} magnetization as the primary remanence.

Thermal demagnetization results from lava samples (sixteen inclination groups) yield a mean ($I_T = 48.6^\circ \text{ }^{+7.0^\circ}_{-10.6^\circ}$; table S5) similar to that calculated from the AF data ($I_{AF} = 50.0^\circ \text{ }^{+7.3^\circ}_{-10.6^\circ}$, for 14 inclination units, excluding the uppermost lava flows; fig. S2P). The estimated angular dispersion of the thermal demagnetization data ($S_F = 18.4^\circ \text{ }^{+6.9^\circ}_{-3.7^\circ}$) is slightly higher than that expected from global lava flow data (16) (Fig. 2). The inclination average from AF demagnetization of sediment samples ($I_{AF} = 54.7^\circ \text{ }^{+3.1^\circ}_{-6.4^\circ}$) (12, 14) is confirmed by thermal demagnetization ($I_T = 53.2^\circ \text{ }^{+5.0^\circ}_{-11.4^\circ}$), and is somewhat steeper than the basalt mean.

Paleolatitude history. The inclination groups, averaged by site, form a progressive sequence of decreasing paleolatitudes with time (Fig. 3) that is inconsistent with the fixed-hotspot hypothesis. We did not recover coral reef material north of Koko Guyot (nor find evidence of such material as sedimentary debris). This is consistent with the idea that the hotspot was once located farther north, beyond the latitudinal zone supporting reef growth (22).

Four data sets are now available from Detroit Seamount based on thermal demagnetization (Fig. 3). Lava emplacement may have been less frequent at Site 884 relative to the other sites due to its flank position. The Site 1204 (Hole B) lavas record a low angular dispersion, but these rocks might carry a CRM, explaining the agreement of their mean inclination with that of the Site 884 basalt section and

the Site 1203 sediments. Because of potential inclination shallowing, the mean inclination from the Site 1203 sediments should be a minimum. This suggests further that the mean derived from the basalts at the same site is shallower because the available lavas underrepresent higher inclination values.

We consider two scenarios; one in which the paleomagnetic results from the Site 884 basalts, 1204 (Hole B) basalts and Site 1203 sediments best represent the field (paleolatitude model A, $I_T = 56.5^\circ \text{ }^{+12.4^\circ}_{-12.6^\circ}$, $N = 3$) and another in which we combine all the individual basalt inclination units from Detroit Seamount into a mean ($I_T = 52.9^\circ \text{ }^{+3.7^\circ}_{-6.9^\circ}$, $N = 32$) (Model B). Using either model, the paleolatitude and age data yield average rates (Model A: $57.7 \pm 19.2 \text{ mm yr}^{-1}$; Model B: $43.1 \pm 22.6 \text{ mm yr}^{-1}$) that are consistent with the hypothesis that the Hawaiian hotspot moved rapidly southward from 81 to 47 Ma (10). The values are consistent with updated estimates of hotspot motion based on independent relative plate motions (5). Both paleolatitude models suggest that most of the motion occurred at times older than the time of the Hawaiian-Emperor bend (Model A, $> 44 \text{ Ma}$; Model B, $> 43 \text{ Ma}$). This is further supported by the mean paleolatitude value from Koko Seamount (based on both thermoremanent magnetizations and CRMs) that is only 2.5° north of the fixed hotspot prediction.

Modeling of Hotspot Motion. Crust ages available from marine magnetic anomalies, radiometric age data from drill sites and geochemical data (23), indicate that the Hawaiian hotspot was close to a spreading ridge during the formation of Detroit Seamount (24). Hence asthenospheric channeling of the plume (e.g. 25) from a position to the south toward a more northerly ridge could have played some role in the difference between the paleomagnetic data and the prediction of the fixed hotspot model. The monotonic age progression of lavas recovered from Detroit to Koko Seamounts, however, leads us to believe that this potential channeling of plume material was limited to the region at, or north of Detroit Seamount. Furthermore, the similarity of the Hawaiian-Emperor chain with the Louisville chain of the South Pacific argues against asthenospheric channeling as the sole cause of the paleolatitude progression.

We examine whether the observed paleolatitude motion can be explained by a geodynamic model of the interaction of a plume with large scale mantle flow. The flow calculation (26) requires a mantle density and viscosity model and a surface velocity boundary condition (14). A tomography model is used to infer mantle density variations (27) and a viscosity structure based on an optimized fit to the geoid (with additional constraints from heat flow) (28) is employed. Both moving and fixed (29–30) plume sources that originate at the top of the low-viscosity layer at the base of the mantle are considered (14).

Fast motion occurs when a conduit is sheared and tilted in the large-scale flow and the tilted conduit rises to the surface aided by a large-scale upwelling. Thus, in these models, fast hotspot motion correspond to slower mantle flow rates (~ 10 to 20 mm yr^{-1}). Most computations (26) yield a hotspot

motion of $5\text{--}10^\circ$ towards the south to southeast during the past 100 million years. It is possible to achieve a good fit to the paleomagnetic data, because the age of the initiation of the Hawaii hotspot is unknown (and can hence be used as a free parameter). For the moving source model, southward motion tends to be faster if an earlier plume origin is assumed. However, plume initiation ages from 180 Ma to 120 Ma (which imply the significant subduction of volcanic edifices older than the oldest extant seamount, Meiji guyot) generally yield the best fits. For the fixed source model, the computed hotspot motion consists of two distinct phases. During the first phase, which lasts 100–150 m.y., southward motion can be rapid. The second phase begins when the first conduit elements that arise from the fixed source reach the surface. The computed hotspot motion is slow during the second phase and, in the example shown (Fig. 4), somewhat toward the north (14).

Overall, the results of the large-scale flow modeling approach described above are consistent with the Leg 197 paleomagnetic data. Potentially important differences are in the total motion predicted since $\sim 80 \text{ Ma}$ [14], and in the need in the modeling results for a change in plate motion at or near the time of the bend. A plate motion change is not required by the paleomagnetic data, although a small change is not excluded.

Implications of Hotspot Motion. The hotspot motion defined by the new paleomagnetic and radiometric age data has implications for a wide variety of issues, including true polar wander (TPW) (31), the morphology of the past geomagnetic field, and the history of plate motions. Some investigators (e.g. 32) have proposed that as much as 30° of TPW (rotation of the entire solid earth) has accumulated during the last 200 million years. But a fixed hotspot reference frame is used to define TPW in these studies. The data presented here, together with other tests (e.g. 33–34), indicate TPW has been overestimated; the Earth has been relatively stable with respect to the spin axis since the Early Cretaceous. Similarly, some changes in the morphology of the geomagnetic field with time (35) that have relied on fixed hotspots to anchor data from global sites are probably artificial. One recent analysis that has not relied on the fixed hotspot reference frame has called for a significant axial octopole contribution (g^3_0) to the time averaged field [36]. This conclusion is controversial, but if correct it would imply that our paleolatitude calculations underestimate the true hotspot motion.

Backtracking the position of early Tertiary and older Pacific basin sites, an essential aspect of some paleoclimate and tectonic studies, requires rethought as prior efforts have also relied on fixed hotspots. The northerly position of the Late Cretaceous Hawaiian hotspot (24) casts doubt on the southern option for the Kula-Farallon ridge [a plate configuration that is typically called upon to create high rates of northward transport for tectonostratigraphic terranes in Alaska and British Columbia (37–38)].

The fixed hotspot interpretation of the Hawaiian-Emperor bend implies that huge plates can undergo large changes in

direction rapidly. But such changes cannot be associated with internal buoyancy forces (e.g. subducting slabs) because these require many millions of years to develop. This has led to the suggestion that plate boundary forces might be responsible (39). The new paleolatitude and radiometric age data (9) suggest that changes of plate motion at the time of the Hawaiian-Emperor bend were much smaller and more gradual than previously thought. Given the central role the Hawaiian-Emperor bend has played as an example of plate motion change, these observations now question whether major plates can undergo large changes in direction rapidly, and whether plate boundary forces alone can play a dominant role in controlling plate motion.

The similarity of the Hawaiian and Louisville hotspot tracks implies that the motion we are tracking by the new paleomagnetic data is of large scale. This Late Cretaceous to early Tertiary episode of hotspot motion was not isolated; motion of the Atlantic hotspots relative to those in the Pacific occurred at similar rates during mid-Cretaceous times (40). These data sets indicate a much more active role of mantle convection in controlling the distribution of volcanic islands. At times, it is this large scale mantle convection that is the principal signal recorded by hotspot tracks.

References and Notes

1. J. T. Wilson, *Canadian Jour. Physics* **41**, 863 (1963).
2. W. J. Morgan, *Nature* **230**, 42 (1971).
3. P. Molnar, T. Atwater, *Nature* **246**, 288 (1973).
4. P. Molnar, J. Stock, *Nature* **327**, 587 (1987).
5. C. A. Raymond, J. M. Stock, S. C. Cande, in *The History and Dynamics of Global Plate Motions*, vol. 121 of *Geophysical Monograph Series*, M. A. Richards, R. G. Gordon, R. D. van der Hilst Eds. (American Geophysical Union, Washington, DC, 2000), p. 359.
6. V. DiVenere, D. V. Kent, *Earth Planet. Sci. Lett.* **170**, 105 (1999).
7. T. Atwater, in *The Eastern Pacific Ocean and Hawaii*, vol. N of *The Geology of North America*, E. L. Winterer, D. M. Hussong, R. W. Decker, R. W. Eds. (Geological Society of America, Boulder, CO, 1989), pp. 21–72.
8. I. O. Norton, *Tectonics* **14**, 1080 (1995).
9. W. D. Sharp, D. A. Clague, *EOS, Trans. Am. Geophys. Union* **83**, F1282 (2002).
10. J. A. Tarduno, R. D. Cottrell, *Earth Planet. Sci. Lett.* **153**, 171 (1997).
11. M. Kono, *Init. Rep. Deep Sea Drill. Proj.* **55**, 737 (1980).
12. J. A. Tarduno et al., *Init. Rep., Proc. Ocean Drill Prog.* (Ocean Drilling Program, College Station, TX, 2002), vol. 197.
13. R. D. Mueller, W. R. Roest, J.-Y. Royer, L. M. Gahagan, J. G. Sclater, *J. Geophys. Res.* **102**, 3211 (1997).
14. Material and methods are available as supporting material on Science Online.
15. P. L. McFadden, A. B. Reid, *Geophys. J.R. Astron. Soc.* **69**, 307 (1982).
16. P. L. McFadden, R. T. Merrill, M. W. McElhinny, S. Lee, *J. Geophys. Res.* **96**, 3923 (1991).
17. A. V. Cox, *Geophys. J.R. Astron. Soc.* **20**, 253 (1970).
18. J. A. Tarduno, *Geophys. Res. Lett.* **17**, 101 (1990).
19. W. A. Berggren, D. V. Kent, C. C. Swisher III, M.-P. Aubry, *S.E.P.M. (Soc. Sediment. Geol.) Spec. Publ. No. 54* (1995), p. 129.
20. R. A. Fisher, *Proc. R. Soc. London A* **217**, 295 (1953).
21. G. B. Dalrymple, M. A. Lanphere, D. A. Clague, *Init. Rep. Deep Sea Drill Proj.* **55**, 659 (1980).
22. J. McKenzie, D. Bernoulli, S. O. Schlanger, *Init. Rep. Deep Sea Drill Proj.* **55**, 415 (1980).
23. R. A. Keller, M. R. Fisk, W. M. White, *Nature* **405**, 673 (2000).
24. R. D. Cottrell, J. A. Tarduno, *Tectonophysics* **362**, 321 (2003).
25. C. J. Ebinger, N. H. Sleep, *Nature* **395**, 788 (1998).
26. B. Steinberger, *Geochem. Geophys. Geosyst.* **3**, 10.1029/2002GC000334 (2002).
27. T. W. Becker, L. Boschi, *Geochem. Geophys. Geosys.* **3**, 10.129/2001GC000168 (2002).
28. B. M. Steinberger, A. R. Calderwood, paper presented at European Geophysical Society XXVI General Assembly, Nice, France, 25–30 March 2001.
29. A. M. Jellinek, M. Manga, *Nature* **418**, 760 (2002).
30. A. Davaille, F. Girard, M. Le Bars, *Earth Planet. Sci. Lett.* **203**, 621 (2002).
31. P. Goldreich, A. Toomre, *J. Geophys. Res.* **74**, 2555 (1969).
32. J. Besse, V. Courtillot, *J. Geophys. Res.* **107**, 10.1029/2000JB000050 (2002).
33. J. A. Tarduno, A. V. Smirnov, *Earth Planet. Sci. Lett.* **184**, 549 (2001).
34. J. A. Tarduno, A. V. Smirnov, *Earth Planet. Sci. Lett.* **198**, 5533 (2002).
35. R. A. Livermore, F. J. Vine, A. G. Smith, *Geophys. J.R. Astron. Soc.* **79**, 939 (1984).
36. R. Van der Voo, T. H. Torsvik, *Earth Planet. Sci. Lett.*, **187** 71 (2001).
37. D. C. Engebretson, A. V. Cox, R. G. Gordon, *GSA Spec. Pap.* **206** 1-59, (1985).
38. H.-P. Bunge, S. P. Grand, *Nature* **405**, 337 (2000).
39. M. A. Richards, C. Lithgow-Bertelloni, *Earth Planet. Sci. Lett.* **137**, 19 (1996).
40. J. A. Tarduno, J. Gee, *Nature* **378**, 477 (1995).
41. This research used samples provided by ODP, which is sponsored by the US National Science Foundation (NSF) and participating countries under management of Joint Oceanographic Institutions Inc. We thank the scientific and operational parties of Leg 197 for their contributions at sea, and the staff of ODP-Texas A&M University for their technical support. Funding for this research was provided by NSF. We also thank Pavel Doubrovine, Gwen Olton, Dan Sinnott and Allyson O'Kane for assistance with magnetic measurements.

Supporting Online Material

www.sciencemag.org/cgi/content/full/1086442/DC1
Materials and Methods
Figs. S1 and S2

5 May 2003; accepted 8 July 2003

Published online 24 July 2003; 10.1126/science.1086442

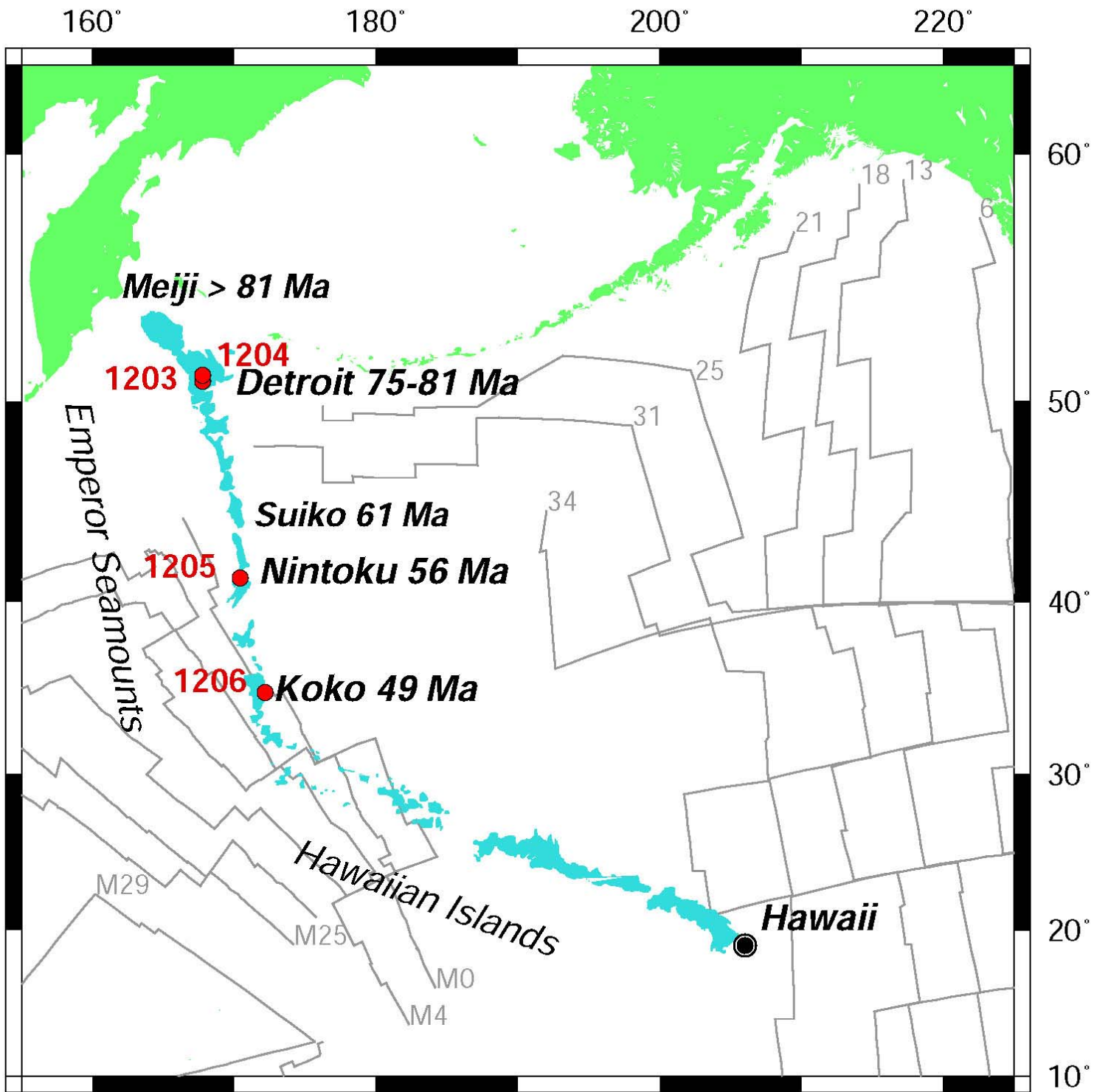
Include this information when citing this paper.

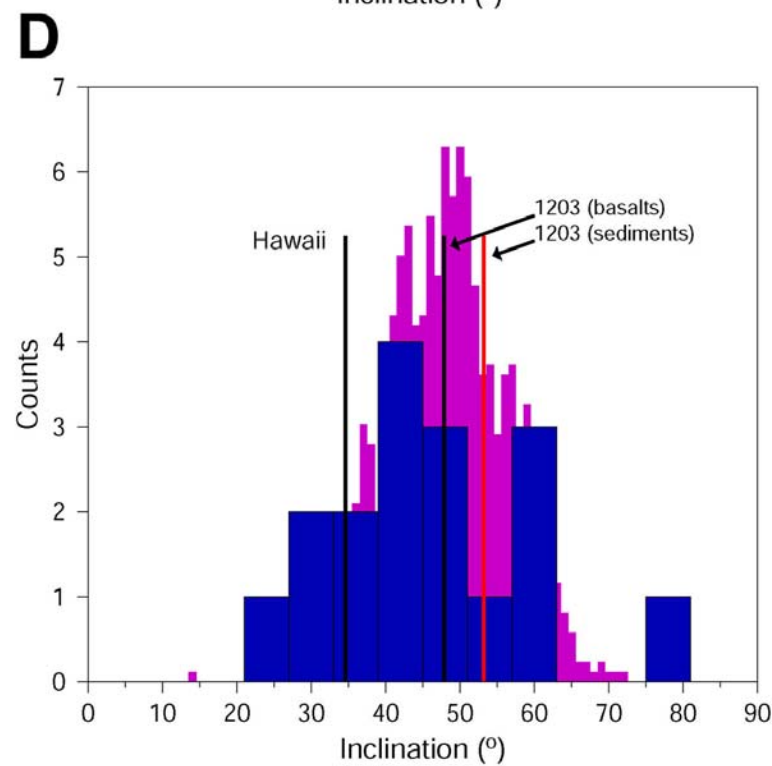
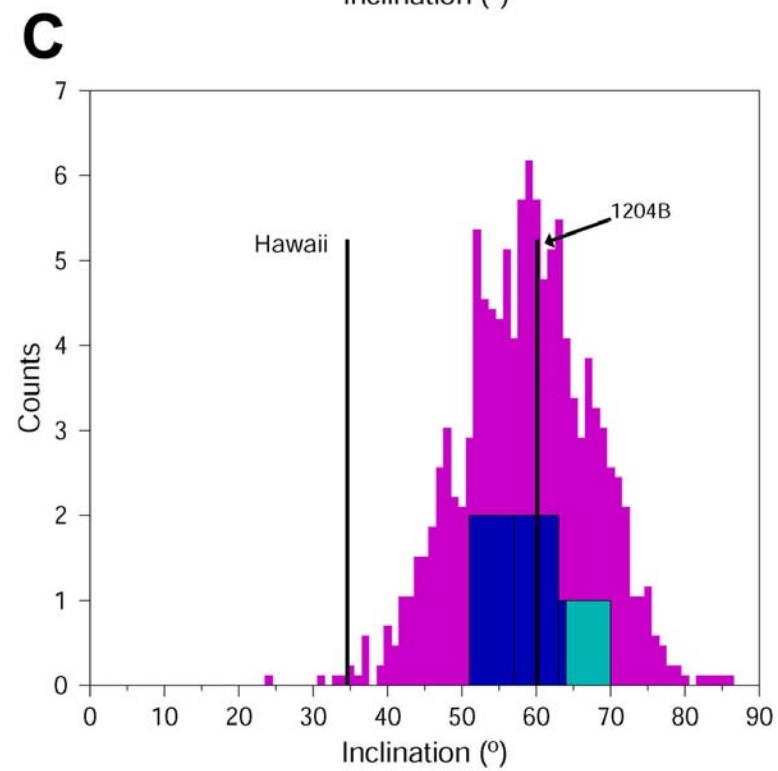
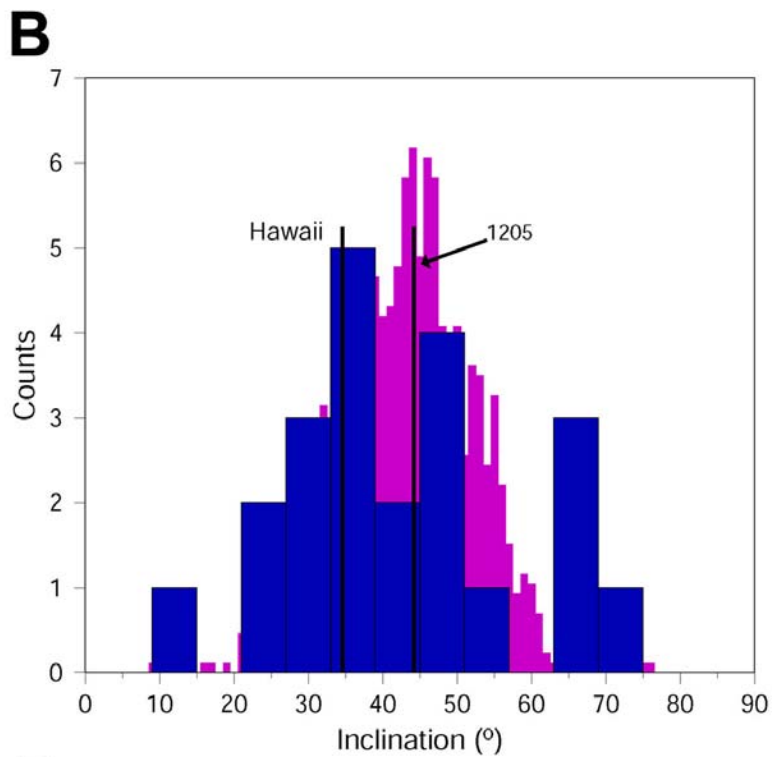
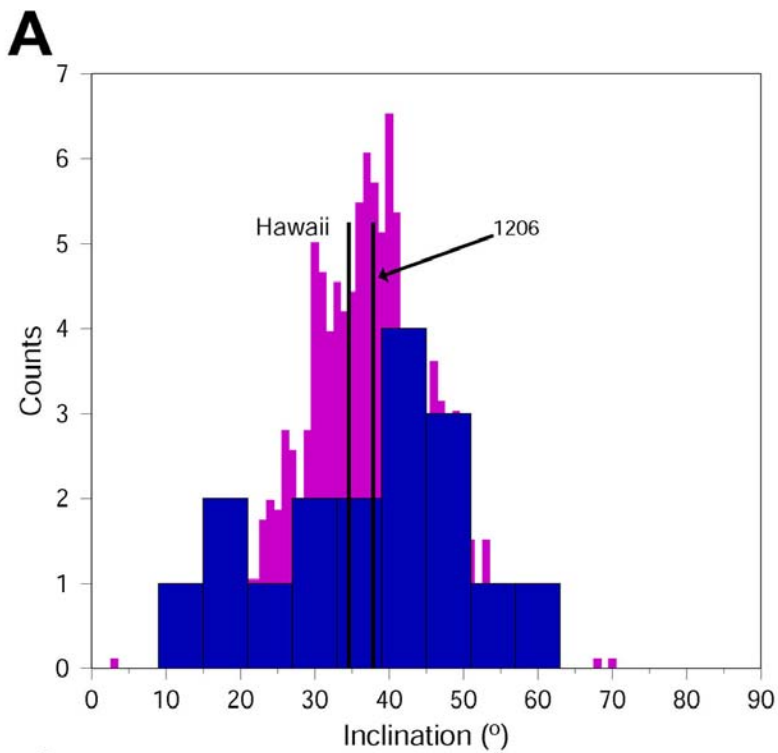
Fig. 1. Hawaiian-Emperor chain shown with Ocean Drilling Program Leg 197 sites (12) and marine magnetic anomaly identifications (13).

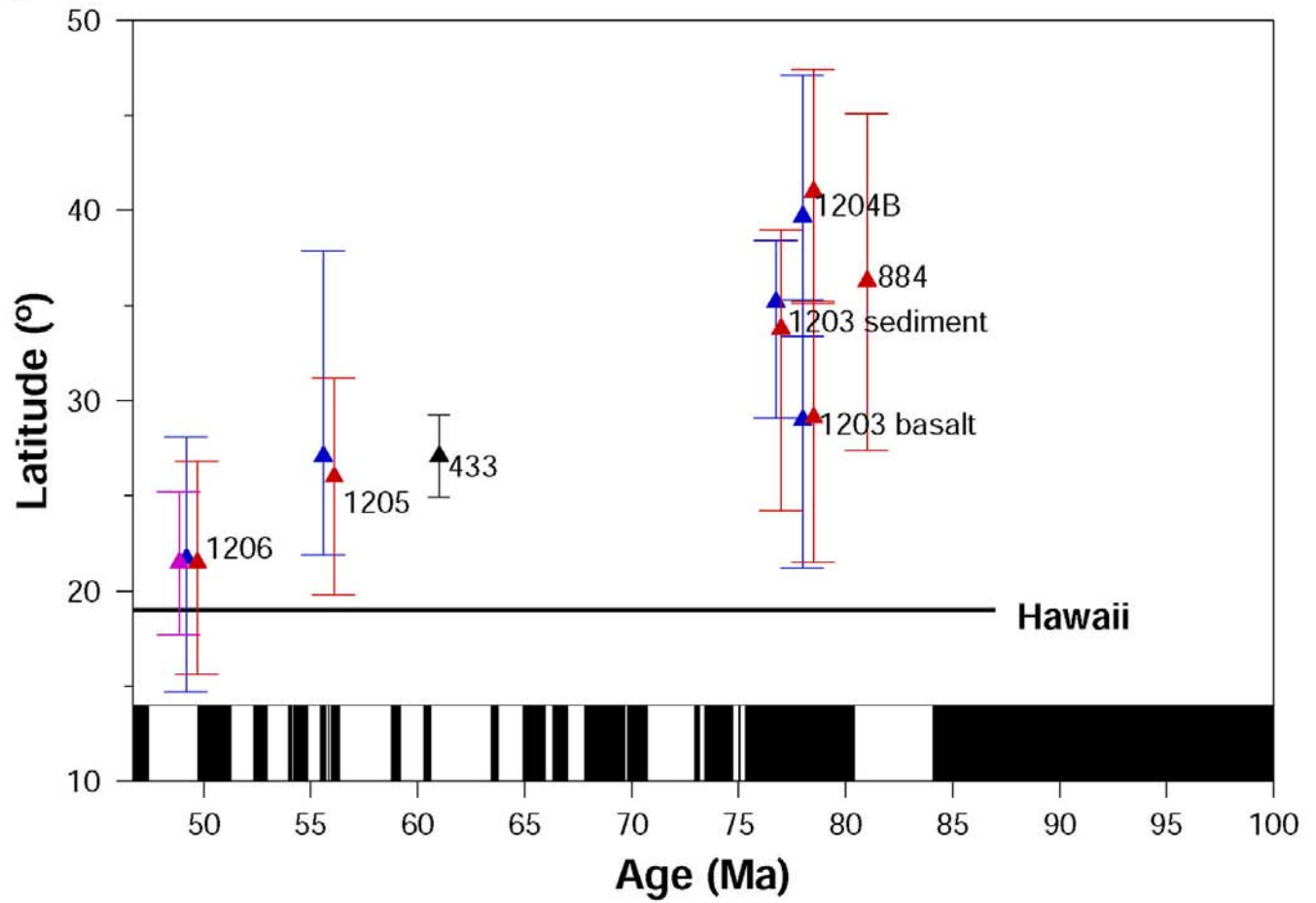
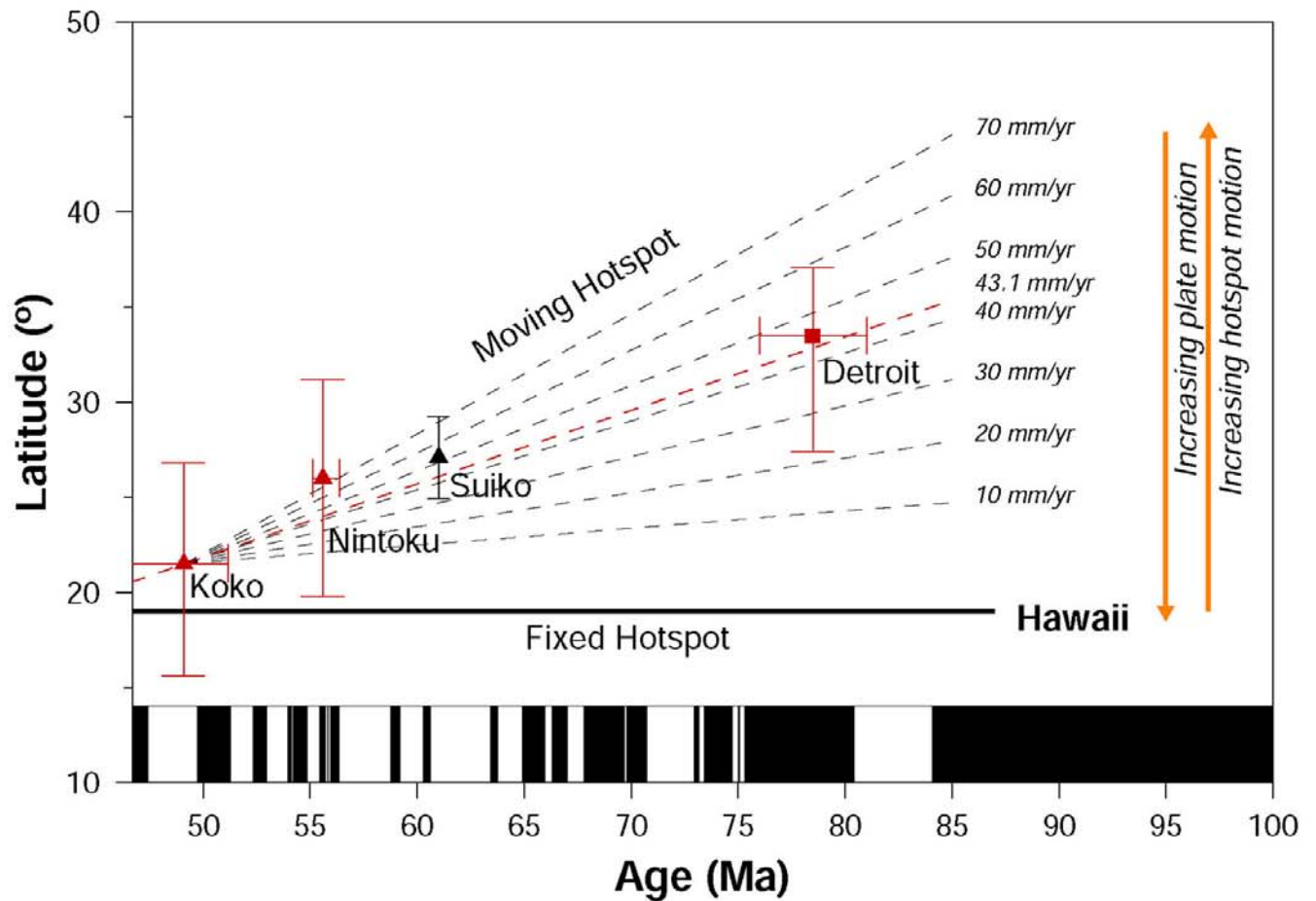
Fig. 2. Paleomagnetic inclination groups for Sites 1206 (A), 1205 (B), 1204 (C), and 1203 (D), based on thermal demagnetization data (blue) shown versus a synthetic Fisher distribution (purple) having the same mean as the experimental data and a dispersion predicted by global lava data (16). Latitude of Hawaii and mean sediment inclination value for Site 1203 (D) are also shown.

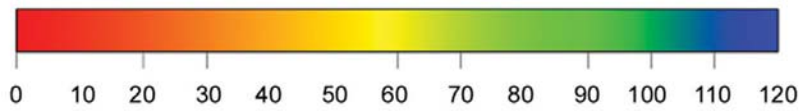
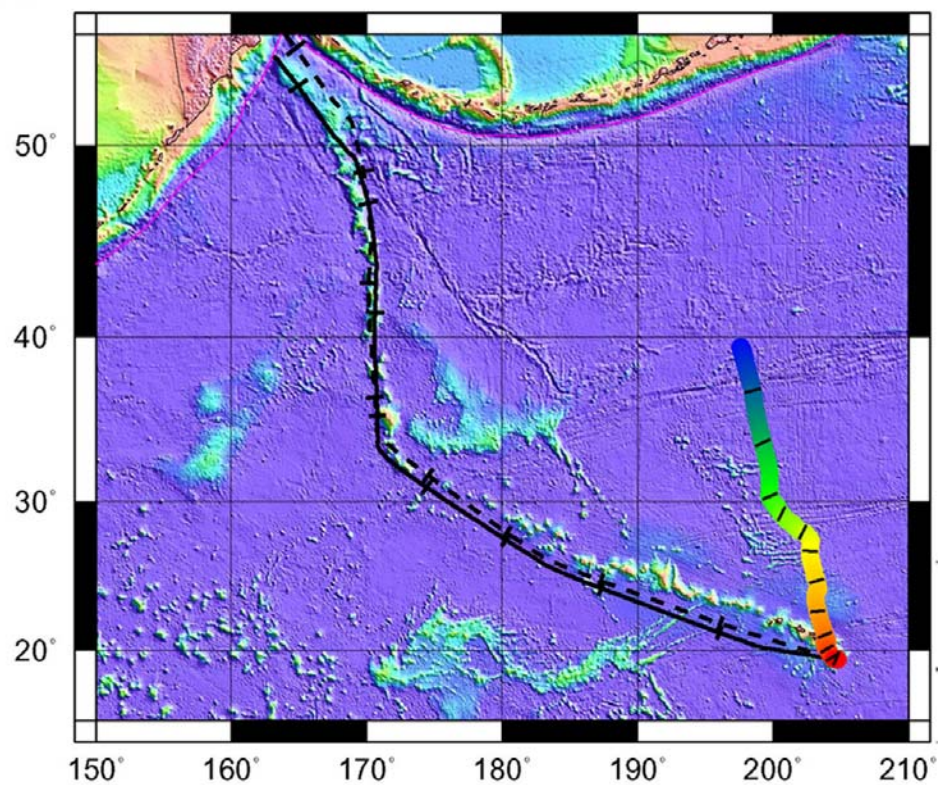
Fig. 3. (A) Paleolatitude data from ODP Leg 197 sites (1206, Koko Seamount; 1205, Nintoku Seamount; 1204B and 1203, Detroit Seamount), ODP Site 884 (Detroit Seamount) (10), and DSDP Site 433 (Suiko Seamount) [11]. Red: results of thermal demagnetization; blue: results of alternating field demagnetization. Result from 433 is based on AF and thermal data. Magenta: magnetization carried by hematite from weathered basalt from Site 1206. (B) Average paleolatitude value for Detroit Seamount (square) based on inclination groups derived from basalts of Sites 884, 1203 and 1204B (Model B, see text) plotted with select values from other seamounts (see A). Also shown is a least squares fit to the data (red) and several paleolatitude trajectories representing combinations of plate and hotspot motion.

Fig. 4. (A) Computed changes of hotspot latitude for fixed-source plume model [14] (continuous red lines) for plume initiation ages of 150, 160 and 170 Ma (upper to lower). Moving source model (14) results (dashed purple lines) are shown for plume initiation at 180, 170 and 160 Ma (upper to lower). Paleolatitude means for Koko, Nintoku, Suiko and Detroit Seamounts (see Fig. 3) are also shown. (B) Computed Hawaiian hotspot motion for fixed-source model (colored line), and tracks for fixed (continuous line; plume initiation at 160 Ma) and moving (dashed line; plume initiation at 170 Ma) source models. Tickmark interval is 10 Ma for both.

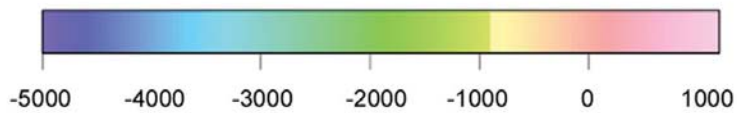




A**B**

A

Time (Ma)



Topography (m)

B